

# Auto-Encoder Optimized PAM IM/DD Transceivers for Amplified Fiber Links

AMIR OMIDI<sup>1</sup>, MAI BANAWAN<sup>2</sup>, ERWAN WECKENMANN<sup>1</sup>,  
BENOÎT PAQUIN<sup>1</sup>, ALIREZA GERVAND<sup>1</sup>, ZIBO ZHENG<sup>1</sup>, WEI SHI<sup>1</sup>,  
MING ZENG<sup>1</sup>, AND LESLIE A. RUSCH<sup>1\*</sup>

<sup>1</sup>Université Laval, Electrical and Computer Engineering Department, Centre for Optics, Photonics, and Lasers (COPL), Québec, Québec G1V 0A6, Canada

<sup>2</sup>Alexandria University, Electrical Engineering Department, Alexandria 21544, Egypt

\*[rusch@gel.ulaval.ca](mailto:rusch@gel.ulaval.ca)

**Abstract:** We examine pulse amplitude modulation (PAM) for intensity modulation and direct detection systems. Using a straight-forward, mixed noise model, we optimize the constellations with an autoencoder-based neural network (NN), an improve required signal-to-noise ratio of 4 dB for amplified spontaneous emission (ASE)-limited PAM4 and PAM8, without increasing system complexity. Performance can also be improved in O-band wavelength division multiplexing system with semiconductor optical amplifier amplification and chromatic dispersion. We show via simulation that for such a system operating at 53 Gbaud, we can extend the reach of PAM4 by 10-25 km with an optimized constellation and a NN decoder. We present an experimental validation of 4 dB improvement of an ASE-limited PAM4 at 60 Gbaud using an optimized constellation and a NN decoder.

© 2024 Optical Society of America under the terms of the [OSA Open Access Publishing Agreement](#)

## 1. Introduction

Within the domain of optical communication, intensity modulation and direct detection (IM/DD) systems are exploited for their simplicity and cost-effectiveness. These systems are commonly found in metropolitan area links (distances less than 80 km), but also play a pivotal role in data centers, ranging from short-reach intra-data-center links (below 300 m) to inter data-center links (between 20 and 80 km). This modulation can also be found in mobile 5G networks, cloud computing infrastructures, real-time augmented reality applications, and the emerging domain of autonomous vehicles, among others [1].

Short reach applications require either an optical transmitter with high output power or an optical receiver with high sensitivity. Pre-amplified receivers have been widely adopted to increase the sensitivity, e.g., for passive optical networks (PONs) [2]. In [3], a single shared semiconductor optical amplifier (SOA) acted in the downstream as a booster amplifier and in the upstream as a pre-amplifier to achieve 50 Gb/s transmission over 50 km distance. Amplification with a SOA can also be useful in integrated photonics to compensate the insertion loss of external modulators [4]. We therefore turn our attention to amplified IM/DD links.

Amplification inevitably introduces signal-dependent amplified spontaneous emission (ASE) noise. The square law detection of ASE in IM/DD leads to non-Gaussian noise statistics. A few solutions have been proposed to improve the receiver sensitivity of amplified pulse amplitude modulation (PAM) IM/DD systems [5, 6]. Based on an approximate analytical model for non-Gaussian and signal-dependent noise, unevenly spaced PAM levels and decision thresholds were found in [5] via an iterative algorithm. They considered only a memoryless channel and their approach is less effective in channels with chromatic dispersion. An experimental feedback method was adopted in [6] to optimize the intensity levels and decision thresholds of amplified PAM4 at 1310 nm where the chromatic dispersion is zero.

As baud rates increase, the effect of chromatic dispersion (CD) becomes critical. With coherent

detection, this deterministic impairment can be easily corrected using receiver side filtering. With direct detection, CD induces a fading effect that can only be slightly countered with receiver side minimum mean-squared error (MMSE) filtering. While the O-band has 1310 nm with zero dispersion in standard single mode fiber (SMF), increasing capacity with multiple O-band wavelengths will lead to limited propagation distances due to fading.

We propose the use of machine learning techniques to jointly optimize the PAM constellation and detector in a system with both amplification and CD. The nonlinear processing in a neural network (NN) decoder can be trained to respond to the square law detection of CD effects and ASE noise. Machine learning has been used to address several other challenges in IM/DD systems, owing to its capability to effectively model intricate relationships. For example, machine learning was exploited for non-linear pre-distortion in [7] and signal equalization in [8]. The end-to-end learning framework was also adopted by [9–12] for IM/DD systems.

Specifically, fiber dispersion was addressed with an autoencoder (AE) for IM/DD in [9], where the primary impairment was inter-symbol interference (ISI). Their system was not amplified. The authors used multiple instances of identical NN structured with feed forward neural network (FFNN); it introduced a substantial computational burden. The FFNN in [9] was replaced with a sliding window bidirectional recurrent network (SBRNN) in both the AE encoder and decoder [10]. Despite the removal of repeated neural networks in the encoder, concerns remained about the cost efficiency of the new recurrent neural network (RNN)-based structure. In [12], they focused on resilience to dispersion variations using end-to-end learning for an IM/DD system; the AE consists of three layers each for the encoder and decoder, featuring hidden layers with (128, 128, 48) neurons. In another study [11], artificial NNs were used to jointly optimize probabilistic shaping and geometric shaping for 50 Gbaud IM/DD. This end-to-end deep learning structure was only considered for the transmitter side.

Although previous research has utilized AEs to tackle diverse impairments in IM/DD systems, to the best of our knowledge, none of these studies has specifically delved into alleviating the influence of ASE noise in amplified links with dispersion. The existing AE models often exhibit elevated complexity, while we are interested in solutions with no added complexity, or moderate complexity justified by significant performance improvement. We improve on existing solutions that do not employ machine learning [5, 6] by finding better decision thresholds that account for nonlinear system behavior. For systems with memory (particularly CD), replacing a threshold with a moderate complexity nonlinear NN receiver can significantly extend reach.

We investigate two channel scenarios. For both cases the encoder is used only to identify nonuniform PAM levels; the encoder computation is done once. For the memoryless channel, the decoder portion is used only to identify threshold levels; the decoder computation is done once. For a channel with memory, the decoder is trained and retained as a detector in lieu of thresholds.

In our first channel, we address a combination of ASE (introduced just prior to photodetection) and detector thermal noise. For this memoryless case, we achieve a 4 dB improvement in an ASE-limited system for both PAM4 and PAM8. In the second scenario, we consider a channel with memory due to CD. The system includes a SOA pre-amplifier and four occupied wavelengths, each with distinct levels of CD. By employing an optimized constellation and an NN detector, at 53 Gbaud we can enhance the reach of PAM4 by 10-25 km. An experimental validation of our model is conducted in an ASE-limited PAM4 system at 60 Gbaud, resulting in a 4 dB improvement.

The structure of the paper is as follows. Section 2 presents end-to-end learning and its application to transceiver optimization. In Section 3, we optimize the transceiver within the framework of a simple model of a mixture of ASE and thermal noise. Section 4 examines transceiver optimization of PAM IM/DD links with SOA pre-amplification. Section 5 discusses the complexity of the deep learning model, drawing comparisons with conventional methods. We present an experimental validation in Section 6 for the memoryless channel case. Finally,

Section 7 provides concluding remarks.

## 2. End-to-end learning for transceiver optimization

We employ end-to-end learning via AEs, leveraging deep neural networks (DNNs). The AE has three primary components: the *encoder* DNN, the *code* layer, and the *decoder* DNN. In communication systems, the encoder generates symbol constellations, while the decoder makes symbol decisions. The schematic representation of the general AE structure adapted for a communication system is illustrated in Fig. 1. We tailor the neural network (NN) structures to suit the specific requirements of the communication channel.

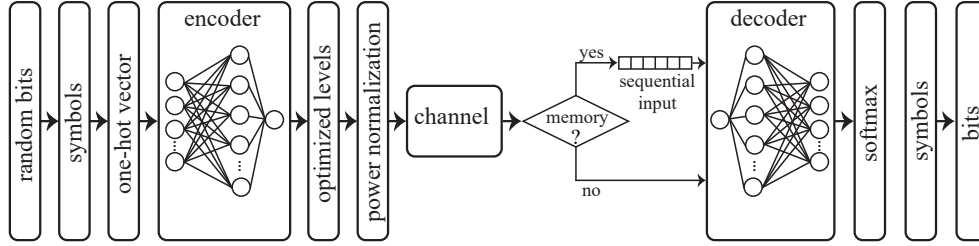


Fig. 1. Block diagram an autoencoder (AE) for communications systems

The initial step converts random bits into symbols via a Gray mapping. Symbols are input to the encoder NN as one-hot vectors, and we will minimize the symbol error rate (SER) to find optimal NN weights. We examine encoder neural networks (NNs) with a feed-forward architecture. Given the nature of our system, there is no need of complicated RNN, long short term memory (LSTM), etc. The output of the encoder are signal levels; they are normalized to unit power and form the AE code layer.

Channel impairments are introduced to the code layer. A memoryless non-Gaussian noise channel will be examined in Section 3, whereas a channel with memory will be considered in Section 4. The decoder operates on the noisy code layer to reconstruct the original data. The decoder outputs a scores vector  $\vec{r}$  and symbol decisions are formed via the Softmax function

$$S(r_i) = \frac{e^{r_i}}{\sum_{j=1}^M e^{r_j}}, \quad (1)$$

where  $r_i$  represents the  $i^{th}$  entry in the scores vector  $\vec{r}$ . This transforms the scores into symbol probabilities; the detector selects the symbol with the highest probability. The symbol decision and the transmitted symbol are used to calculate the loss, i.e., the cross entropy between them. The weights of the encoder and decoder are updated through the back-propagation algorithm. Upon model convergence, we generate random test data to estimate the SER performance.

For a channel with memory, we must modify the decoder. One approach uses dedicated DNNs, e.g., RNN and LSTM to support memory explicitly, while the other modifies the input of the decoder into sequential data windows. For our research, we chose the less computationally complex latter approach. We incorporate a small window size in Section 4 to address the influence of CD. The hyper-parameters of the AE used in the rest of this paper are presented in Table 1.

## 3. Simple mixed noise system

All optical systems are subject to thermal noise during photodetection. For amplified systems, the ASE produced during amplification often dominates thermal noise. The photodetection process

Table 1. Hyper parameters of the AE

Hyper parameter	Value
hidden layers and hidden units	(15,1,1,15)
learning rate	0.05
activation function	CELU
optimizer	Adam
batch size	2048
loss function	CrossEntropyLoss
decoder input sequence size	memoryless = 1, with memory = 5

squares the ASE noise and adds the thermal noise, as illustrated in Fig. 2. Although both the thermal and ASE noise follow Gaussian distributions, the square law process in IM/DD systems leads to the detected noise being a mixture of Gaussian (thermal) and chi-square (photodetected ASE) noise.

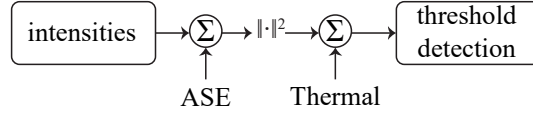


Fig. 2. Memoryless channel model for mixed noise types

We employ a straightforward analytical model to characterize the mixture of different types of noise. The received signal before the photodiode is  $s + N_{\text{ASE}}$ , where  $s$  is the transmitted PAM signal with intensity levels of  $[P_0, P_1, \dots, P_{M-1}]$ . The received signal after photodetection is given by

$$(s + N_{\text{ASE}})^2 + N_{\text{th}}, \quad (2)$$

where  $N_{\text{th}}$  is the thermal additive white Gaussian noise (AWGN) with zero mean and variance  $\sigma_{\text{th}}^2$ . Given  $N_{\text{ASE}}$  is the zero-mean Gaussian random variable with variance  $\sigma_{\text{ASE}}^2$  for optical ASE, the photodetected electrical ASE noise follows a *chi-squared* distribution with one degree of freedom [5, 13].

The detected power attributable to the transmitted signal is given by

$$I^2 = E[(Rs^2)^2] = R^2 E[s^4] = E[s^4], \quad (3)$$

where  $R$  is the photodiode responsivity that is assumed to be 1 A/W. The detected power attributable to noise (see Appendix A for the development) can be expressed as

$$\sigma_N^2 = 4E[s^2]E[N_{\text{ASE}}^2] + E[N_{\text{ASE}}^4] + E[N_{\text{th}}^2] = 4E[s^2]\sigma_{\text{ASE}}^2 + 3\sigma_{\text{ASE}}^4 + \sigma_{\text{th}}^2, \quad (4)$$

where the first variance term is for Gaussian but signal-dependent noise, the second variance term is for chi-square noise, and the third variance term is for Gaussian noise. We note that in the second term we used the result that a standard normal variable has a fourth moment equal to three times its variance.

To assess the relative influence of ASE and thermal noise, we introduce  $\alpha$  as the percentage of total noise attributed to thermal noise that is,

$$\alpha\sigma_N^2 = \sigma_{\text{th}}^2, \quad (5)$$

and

$$(1 - \alpha)\sigma_N^2 = 4\sigma_{\text{ASE}}^2 + 3\sigma_{\text{ASE}}^4, \quad (6)$$

where we assume unit signal launch power ( $E[s^2] = 1$ ).

Consider PAM4 with a received constellation that is equally spaced for noise-free systems, i.e., traditional PAM4. We plot in Fig. 3a the received symbols in the presence of all thermal noise (upper scatter plot) or all ASE noise (lower scatter plot). In the case of all-thermal noise, equally spaced symbols achieve the lowest error rate owing to the nature of the Gaussian distribution. When the noise is all ASE, the square-law detection process significantly alters the noise characteristics. There are noticeably lower noise levels at smaller amplitudes, making tighter spacing at low amplitude desirable. For cases combining of both ASE and thermal noise, the overall distribution of the symbols would be influenced by the mix factor  $\alpha$ .

### 3.1. Optimized constellations and thresholds

We used the AE in Fig. 1 to find PAM4 and PAM8 constellations that minimize SER. The channel box in Fig. 1 was replaced with the operations in Fig. 2. The constellation output by the encoder is normalized to unit average power, i.e.,  $E[s^2] = 1$ . We fix a received signal-to-noise ratio (SNR) and  $\alpha$ , and run the AE to find the optimal constellation for unit transmitted power. We note that although  $E[s^2] = 1$ , the received SNR is proportional to  $E[s^4]$  and will vary with constellations  $[P_0, P_1, \dots, P_{M-1}]$ . The noise power  $\sigma_N^2$  is scaled by  $E[s^4]$  to produce the received SNR under study. This scaled power is used to generate ASE and thermal noise in simulations.

In Fig. 3b, we depict optimized PAM4 constellations with filled circle markers for each  $\alpha$  at a SNR of 18 dB. The empty circle markers at the top of the figure are the standard PAM4 constellation. For the case of all thermal noise ( $\alpha = 100\%$ ), the AE constellation is very similar to standard PAM4, i.e., equally spaced levels. As  $\alpha$  decreases, reflecting scenarios with increasing ASE noise dominance, the constellation points are tightly spaced at lower amplitudes to take advantage of the reduced noise present there.

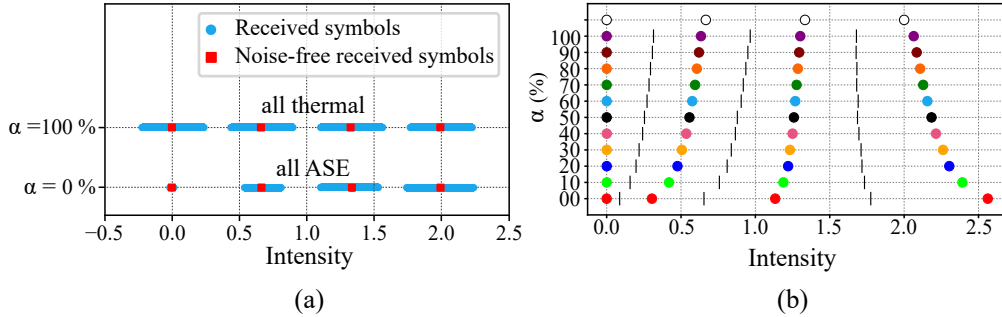


Fig. 3. (a) Received symbols for standard PAM4 for noise that is zero (square markers), all thermal, or all ASE, and (b) optimized constellations for various  $\alpha$  (circles) and their optimized thresholds (vertical lines).

As this idealized channel is memoryless, a one-shot, threshold-based detection is optimal. For standard PAM, the detection threshold is positioned at the midpoint between the constellation points, as it is optimal for Gaussian noise. Midpoint thresholds are no longer optimal for mixed noise. We use the bisection method to determine the thresholds from the AE-decoder. Specifically, for any two given adjacent constellation points, the threshold is initially set to be the midpoint. The next step is to determine which side of the current threshold will lead to improved performance. This can be accomplished by testing two points close to the current threshold, one on each side of the threshold. We set the distance difference between the testing points and current threshold to  $\pm 1e-5$ . We pass the two test points to the AE-decoder, and record the corresponding decisions. If both points are classified to the same constellation point by the AE-decoder, the threshold is updated to the midpoint of the current threshold and the other

constellation point under consideration. This procedure continues until the two test points are classified to distinct constellation points by the AE-decoder. In this case, the current threshold is retained.

The same algorithm is iteratively applied to identify thresholds between other adjacent constellation points. These thresholds are presented in Fig. 3b with black vertical lines for constellations at SNR of 18 dB. In Appendix B, we further present the AE-optimized PAM4 and PAM8 constellation and detection thresholds over various SNR levels.

Note that, for a memoryless channel, once the AE finds the constellations and detection thresholds, the AE encoder and decoder can then be discarded. Accordingly, the complexity of the standard and the AE-optimized PAM system is, therefore, identical.

### 3.2. Performance evaluation

We evaluate the SER performance of the AE-optimized PAM4 and PAM8 systems. For each SNR and  $\alpha$ , we find the optimal transceiver (constellation and detection thresholds). We sweep the SNR and run Monte Carlo simulations of the channel in Fig. 2 for each optimized transceiver. We ensure that we count at least 100 errors when estimating the SER, transmitting up to 500,000 symbols.

Figure 4a plots the SER vs. SNR under both PAM8 and PAM4, with PAM8 results in solid lines, and PAM4 results in dashed lines. Each line refers to a specific  $\alpha$  value, and from left to right, the  $\alpha$  value increases by 10%. For any given SER target, i.e.,  $10^{-3}$ , the required SNR increases with  $\alpha$ , indicating that the AE-optimized transceiver could exploit the non-Gaussian nature of the noise.

To quantify the improvement of AE-optimized vis-à-vis standard PAM, we examine the required SNR at SER of  $10^{-3}$ . Fig. 4b depicts the required SNR versus  $\alpha$  under PAM4 and PAM8 for both standard and AE-optimized transceivers. The standard transceiver exhibits an inverse trend as its AE-optimized counterpart, namely, the required SNR declines with  $\alpha$ . This is because the standard transceiver is only optimal under AWGN systems ( $\alpha = 100\%$ ), and inefficient in dealing with mixed thermal and ASE noise or mere ASE noise. Accordingly, the performance gap between the AE-optimized transceiver and standard one peaks at  $\alpha = 100\%$ , and over 4 dB SNR gain is obtained using the AE-optimized transceiver for both PAM4 and PAM8. In the particular case of  $\alpha = 0\%$ , equivalent performance is observed for both transceivers, verifying the optimality of the AE-based solution.

## 4. Amplified PAM IM/DD systems

The performance of a PAM system can be enhanced with a SOA integrated either monolithically or as a hybrid. While IM/DD often relies on directly modulated sources, there is great emerging interest in silicon photonic external modulators [14] due to their compatibility with integrated solutions. In [15], a SOA was used at the transmitter with PAM for data center applications. In [2], a SOA was used at the receiver for PON applications to extend the link budget. Whether located at the transmitter or receiver, the SOA will introduce ASE. The stronger the amplification, the more ASE is added, and it is more beneficial to use the optimized PAM constellations.

### 4.1. Systems with SOA pre-amplification

We present in Fig. 5 the block diagram of an IM/DD PAM system with non-zero dispersion and SOA pre-amplification. We consider a target of 53 Gbaud transmission rate using Nyquist signaling to minimize the occupied bandwidth and neglect ISI. The otherwise ideal modulator is modeled with a 10 dB extinction ratio. Transmission performed over standard SMF. The receiver thermal noise is fixed at -73 dBm. We include signal-dependent shot noise in addition to the chi-square noise from ASE. Without the use of a SOA, this system requires -13 dBm received optical power to achieve a bit error rate (BER) of  $1.8e-4$  for PAM4. We note in passing that

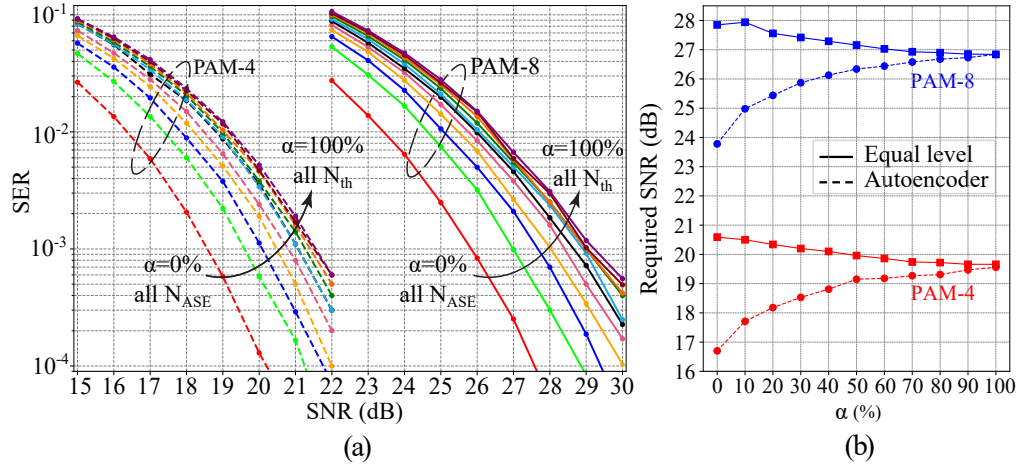


Fig. 4. (a) PAM4 and PAM8 symbol error rate (SER) vs. signal-to-noise ratio (SNR) of AE-optimized transceivers for various  $\alpha$ , and (b) required SNR vs.  $\alpha$  for AE-optimized and standard PAM4 and PAM8 at  $SER=10^{-3}$ .

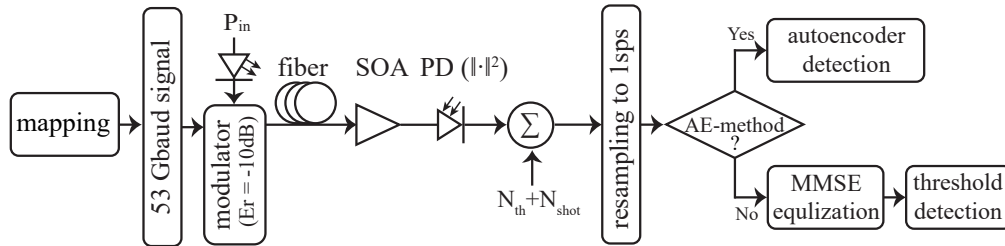


Fig. 5. Block diagram of the amplified IM/DD PAM system with non-zero dispersion

PAM4 and PAM8 have a Grey mapping, so that BER is the SER divided by the number of bits per symbol.

The SOA is simulated in a pre-amplifier configuration, with a noise figure of 6 dB. The SOA gain ranges from 0 to 20 dB. Adjusting SOA gain changes the noise power split between thermal/shot noise and ASE noise (similar to the  $\alpha$  parameter in the previous section). Varying the SOA gain allows us to reduce the required optical power for the target BER. This reduction in the required received power (often termed sensitivity improvement) provides a margin for accommodating various system losses in a practical implementation.

We simulate a four-wavelength, coarse wavelength division multiplexing (WDM) system in the 1300 nm band. For the three wavelengths with non-zero dispersion, the system has memory, unlike the simple system presented in the previous section. To train the AE-optimized constellations, we will use a sequential input version of the decoder seen in Fig. 1. Standard PAM uses a receiver-side, linear equalizer to mitigate losses from chromatic dispersion, followed by threshold detection. Unlike the previous section, we will not use threshold detection for optimized constellations, but instead retain the AE decoder to take advantage of its enhanced capability to combat CD.

#### 4.2. Previous iterative approach for optimization

In [5], constellations and thresholds were optimized for a similar SOA amplified IM/DD PAM system. They used an iterative, numerical approach to find the constellation points sequentially. The first PAM level is transmitted at the lowest intensity permitted by the modulator extinction ratio. The decision threshold is found for a target SER using the probability distribution of the received power, as found by 1) a theoretical approximation at zero dispersion, or 2) Monte Carlo simulations (or experimental measurements) that can include CD effects. They sweep the next PAM symbol level to find one attaining the same SER target when using the previously selected lower threshold. It is a sequential approach: as each symbol level/threshold is fixed, the next is found. At the end of this process, all PAM4 levels and the decision thresholds have been identified.

Consider first a 53 Gbaud back-to-back system employing a SOA with gain of 20 dB. No equalizer is needed, since the system experiences no dispersion. The optimized PAM levels are found via Monte Carlo simulations using the iterative method. Fig. 6a gives a histogram of the sampled received signal, with orange bars showing the decision thresholds. The threshold placements are consistent with equal SER for each type of symbol error.

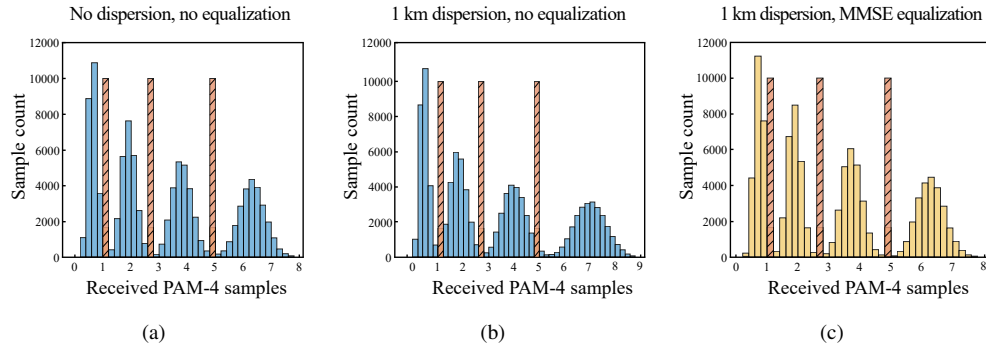


Fig. 6. For an iteratively-optimized constellation, histograms for received signal under a) no dispersion and no receiver-side equalizer, b) 1 km of dispersion at 1250 nm and no equalizer, and c) 1 km of dispersion at 1250 nm and a MMSE equalizer.

Suppose next that we use the same constellation for 1 km transmission at 1250 nm with non-zero dispersion. The histogram in Fig. 6b shows the distortion introduced by the CD. Using the same thresholds would lead to unbalanced SER per error type and degraded performance. In Fig. 6c we use a linear equalizer, compensating for much of the distortion. Compared to Fig. 6a, the distributions have changed in Fig. 6c, and it is not certain that we can reach the target SER.

#### 4.3. Performance comparison of optimized constellations (AE versus iterative)

Equalization cannot be included in the iterative optimization of thresholds and PAM levels: the equalizer can only be calculated once all PAM levels are known, while the iterative method fixes each level sequentially. Our optimization approach allows for the joint optimization of constellations and equalization/detection processes. The sequential inputs to the AE decoder in Fig. 1 enables it to function as both an equalizer and a detector. We examine the performance advantage of the AE optimization.

The coarse WDM O-band system we simulate has signals at 1271 nm, 1291 nm, 1310 nm, and 1331 nm. At the zero-dispersion 1310 nm wavelength, we expect no dispersion and no advantage from the AE approach. This was borne out in our simulations, with similar constellations, threshold and performance for the two optimizations. We ran extensive simulations of all

three non-zero dispersion wavelengths. We present results only for 1291 nm, as the other two wavelengths exhibited similar trends.

For a given fiber length and SOA gain, we run Monte Carlo simulations of PAM4. From the BER vs. received power curves, we extract the required received power to achieve a BER of  $1.8e-4$ . Sensitivity improvement is the difference in dB between this received power and that required for zero fiber length and zero SOA gain (-13 dBm). To facilitate the comparison with the results in the previous section, for each SOA gain we associate an equivalent  $\alpha$ , where  $\alpha$  is the percentage of total noise power attributable to the fixed -73 dBm thermal noise power.

Fig. 7a and b present the sensitivity improvement versus SOA gain at 1291 nm after 1 km and 3 km of fiber propagation, respectively. There is a second upper x-axis with the equivalent  $\alpha$ . Results in green with diamond markers are for the iteratively optimized constellation/thresholds with linear equalization. Results in blue with square markers are for the the AE-optimized constellation and AE decoder.

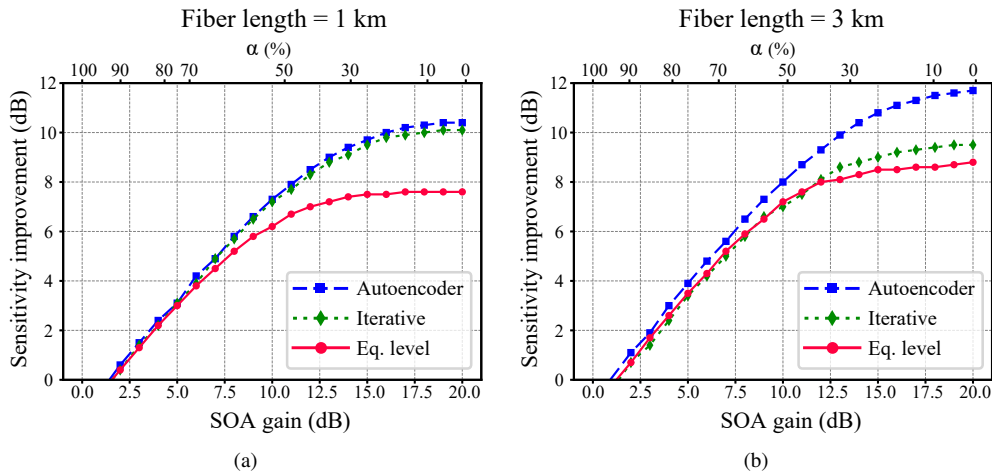


Fig. 7. Sensitivity improvement vs. SOA gain for three PAM4 systems at 1291 nm and fiber length of a) 1 km, and b) 3 km; upper  $x$ -axis give percentage of receiver noise attributable to thermal noise.

Both the iterative and AE approaches outperform standard PAM at short fiber lengths, up to 3 km. Consistent with Section 3, the most significant performance gains vis-à-vis standard PAM are observed at low  $\alpha$  values, i.e., where SOA amplification is high. The AE transceiver shows good improvement at both lengths examined. The iterative approach loses most improvement at the 3 km length. This can be directly attributed to the constellation and thresholds being optimized for zero dispersion. As mentioned previously, the iterative method cannot take into account the receiver-side filtering to combat CD.

To the previous examination of transmission at 1291 nm, we add two other non-zero dispersion wavelengths in the O-band. In Fig. 8 we plot the relative performance with markers to indicate wavelengths. The dashed lines are the improvement of the AE-optimized transceiver vis-à-vis standard PAM, and solid lines are the improvement of the AE-optimized transceiver vis-à-vis iteratively-optimized PAM transceivers [5].

Similar trends are observed for the three non-zero dispersion wavelengths. The improvement of AE over standard PAM transceiver grows with the SOA gain, but remains roughly stable over distance. Under 20 dB SOA gain, 2.7 dB and greater improvement can be achieved at the three wavelengths and three distances considered. In contrast, the improvement over iteratively-optimized PAM transceiver becomes noticeable under longer distance and larger SOA

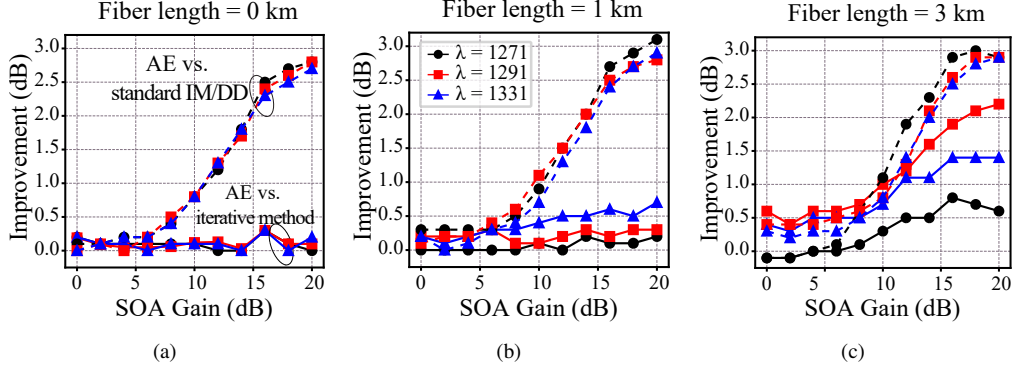


Fig. 8. Improvement obtained by the AE vs. standard IM/DD and the iterative method for the wavelengths of 1271 nm, 1291 nm, and 1331 nm, for the three fiber lengths of (a) 0 km, (b) 1 km, and (c) 3 km for

gain. This shows that as the fiber gets longer, the MMSE equalizer is less effective at correcting CD, while the nonlinear NN remains effective. At 3 km, 0.5 to 2 dB improvement can be obtained for the three considered wavelengths.

At distances exceeding 3 km, neither the standard constellation nor the iterative constellation/thresholds provide recoverable signals due to substantial distortion encountered at a 53 Gbaud transmission rate. In contrast, the AE approach consistently yields performance enhancements, and extends the feasible transmission distances. We fix the SOA gain to 20 dB, and plot in Fig. 9a the sensitivity improvement vs. fiber length for the three non-zero dispersion wavelengths. The dips at 5 km can be attributed to a CD-induced fading, similar to those observed in [9, 10, 16]. The reach extends to 10 km at a wavelength of 1271 nm, approximately 20 km at 1291 nm, and up to 24 km at 1331 nm.

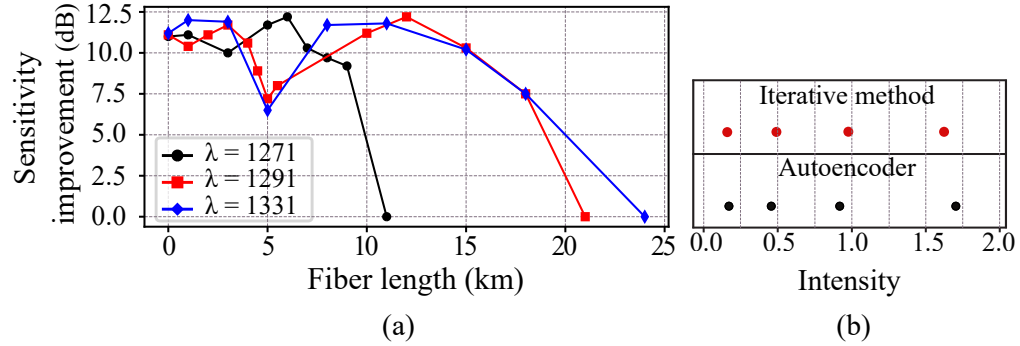


Fig. 9. (a) For SOA gain of 20 dB, sensitivity improvement vs. fiber length for AE-optimized PAM-4 for three non-zero dispersion wavelengths and (b) Constellations obtained using the iterative method and the AE for wavelength of 1291 nm and fiber length of 3 km with SOA gain of 20 dB.

Figure 9b plots the constellations found from the iterative and the AE methods for SOA gain of 20 dB at 1291 nm. The difference between them is apparent. While much of the improvement in reach can be attributed to the AE decoder in combating CD, modification to the constellation also helps.

## 5. Complexity Analysis

In this section, we evaluate the computational complexity of our model and compare it with conventional methods as well as other end-to-end learning methods [9, 10, 12]. For memoryless channels, our end-to-end learning method derives optimized PAM levels and fixed thresholds from the transmitter (encoder) and receiver (decoder) NNs. Once the constellations and thresholds are identified, the NN are discarded. This approach introduces no additional computational overhead during transmission.

For channels with memory, such as systems with ISI resulting from CD, our method can still derive optimized PAM levels from the encoder NN. As before, there is no additional complexity introduced on the transmitter side. To tackle ISI, we implement sequential input processing using a sliding window for the receiver NN. Based on the parameters of our receiver NN shown in Table. 1, the detection process for each received symbol involves  $(5 \times 15) + (15 \times 4) = 135$  multiplications as data passes from the input layer through the hidden layers to the output layer. The decoder uses a continuous exponential linear unit (CELU) activation function, defined as  $\text{CELU}(x) = \max(0, x) + \min(0, \alpha(\exp(x/\alpha) - 1))$  with a default  $\alpha$  value of 1. Additionally, the decoder uses a Softmax( $\cdot$ ) function at the output (vector length equals PAM order). The  $\text{argmax}(\cdot)$  operation is then employed to for symbol estimation.

Conventional approaches use linear filtering and threshold detection for IM/DD systems with memory. The linear filter mitigates the dispersion-induced fading to a limited extent, with longer filters offering little performance improvement no matter the fiber length. Typical number of taps are on the order of 15-20. We used 15 taps in our simulations and 19 taps in our experiments. While NN at 135 multiplications has greater complexity than a filter with 15 multiplications, the added complexity is not excessive. In contrast, previously proposed end-to-end learning models can employ multiple hidden layers, each with tens or hundreds of neurons, in both the encoder and decoder NNs [9–12]. We have avoided such high computation.

## 6. Experimental Validation

We experimentally validated the improvement of AE-optimized constellations in the mixed noise case of Section 3. We examined PAM-4 in an optical system with erbium-doped fiber amplifiers (EDFA) and a silicon photonics external modulator. While our simulations involved a straightforward combination of ASE and thermal noise, the experimental phase introduced additional linear and nonlinear effects from various components. We tested constellations from Fig. 3b for  $\alpha = 0\%$ , 10%, 20%, 30%, 40%. The thresholds in Fig. 3b were not used; experimental data were instead fed to the AE decoder for independent training. After convergence, we extracted the experimental optimal thresholds and discarded the decoder. The  $\alpha = 0\%$  constellation was retained as it yielded the best performance. This is not surprising as the heavily amplified experimental received signal was ASE-limited.

The experimental setup is shown in Fig. 10a. We use a silicon Mach-Zehnder modulator (MZM) for the experimental demonstration, which is designed to operate in the C-band. The modulator consists of 4-mm phase shifters implemented as lateral PN-junctions on both arms for single drive push-pull operation. The MZM has traveling-wave electrodes, providing a 40 GHz electro-optical bandwidth and a  $V_\pi$  of around 8V, by carrier depletion [17]. The length difference between each arm is set to 100  $\mu\text{m}$ , leading to a sinusoidal transmission function at the output of the MZM. Heaters on both arms allow us to finely tune the bias for a fixed source wavelength. We operate at a quadrature point while keeping a low reverse bias voltage on the electrodes to maximize the modulation efficiency. Since the MZM voltage response has a negative slope around the chosen quadrature point, the received power is expected to represent the inverted data sequence (logic zero at the highest power level). A tunable coupler (Mach-Zehnder interferometer) with a heater on each arm is placed before the MZM to allow us to adjust the coupling ratio between modulator

arms to maximize the modulation depth.

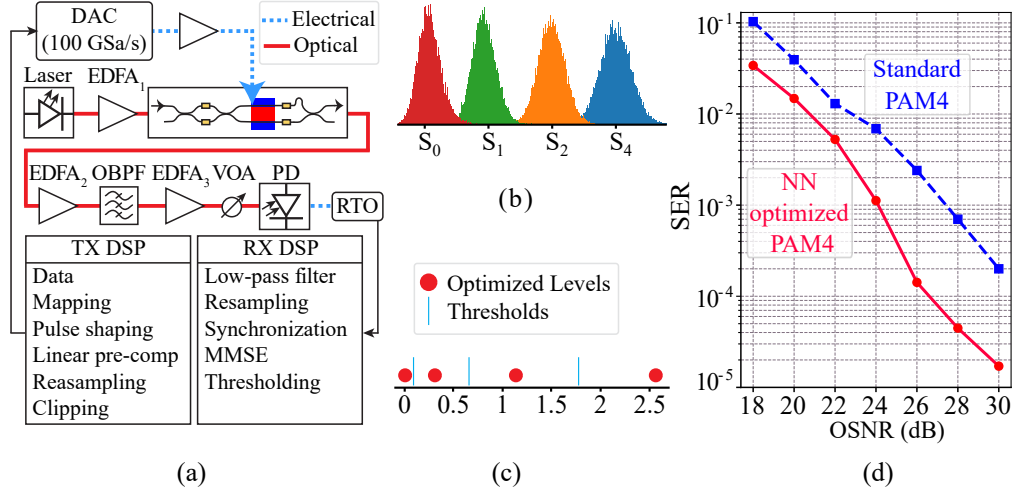


Fig. 10. (a) Experimental setup, (b) conditional probability of received PAM4 symbols, (c) optimized PAM4 levels (unit transmit power), and (d) symbol error rate vs. OSNR.

We generate a random sequence of  $2^{17}$  symbols. We map the symbols to either standard PAM4 or the AE-optimized constellation. We synthesize the 60 Gbaud radio frequency signal with a digital-to-analog convert (DAC) at 100 GSa/s. We amplify the DAC output to 4-V peak-to-peak and send it to the MZM. The MZM input optical power is boosted to 24 dBm by an EDFA to pre-compensate the insertion loss of the chip and to introduce ASE noise. At the receiver side, the optical signal is pre-amplified using another EDFA, increasing the sensitivity, and adding more ASE noise. We use a separate EDFA as a noise source to tune the received optical signal-to-noise ratio (OSNR) from 18 dB to 30 dB. The optical signal is converted to the electrical domain via a 70-GHz bandwidth photodiode and sampled with a 65 GHz real-time oscilloscope at 160 GSa/s.

Knowledge of the transmitted random sequence (no pseudo-random sequences were used) allowed us to isolate receiver noise at each specific PAM level. Fig. 10b plots the conditional probability densities at reception of a standard PAM4 constellation. The highest power PAM level has noise with largest variance; this noise has a significantly longer tail. The differences in mean, variance and distribution for each PAM level is attributable to both the amplification (due to the presence of ASE and signal-dependent shot noise) as well as modulation nonlinearities in the silicon MZM [18]. Figure 10c plots the PAM4 levels found in simulation for all-ASE noise, and the thresholds found from an AE-decoder trained on experimental data.

The same digital signal processing (DSP) stack at transmitter and receiver is used for both standard and AE-optimized PAM4 constellations. The symbols are shaped with a root-raised-cosine pulse with a roll-off factor of 0.1. We use a finite impulse response (FIR) filter to pre-compensate for the frequency response of the DAC and radio frequency (RF) driver. At the receiver side, we apply a MMSE filter with 19 taps at 2 samples per symbol.

The maximum achievable OSNR when operating near the quadrature point is 30 dB in our setup. To sweep OSNR, we load the received signal with additional ASE. In Fig. 10d we plot the SER versus the OSNR in dB. At the maximum OSNR, we achieve almost an order-of-magnitude reduction in SER. The OSNR gain using the AE-optimized constellation is over 4 dB at the high end of the OSNR range examined. The simple act of skewing PAM4 levels per Fig. 10c improves SER above and beyond the performance advantages of optical amplification.

## 7. Conclusion

We have presented a comprehensive examination of the advantages of an AE-optimized transceiver for PAM in amplified IM/DD links. We have examined simple memoryless channels, as well as practical amplified links. For SOA-amplified O-band WDM links with non-zero dispersion, we demonstrated reach extension of 10-25 km via simulation. For an amplified C-band link with limited memory, we demonstrated SER improvement experimentally. The combination of optimized constellation and nonlinear NN decoder enhances IM/DD to higher throughput and/or longer links. The successful adaptation of our method to various channel conditions underscores its versatility and robustness, and the potential of end-to-end learning to transform optical communication systems.

## Appendix A Noise variance calculation

The following is the development of the noise power used in (4). Starting from (2), we find the power of the noise terms per

$$\begin{aligned}
 P_{\text{noise}} &= E[(2sN_{\text{ASE}} + N_{\text{ASE}}^2 + N_{\text{th}})^2] \\
 &= E[4s^2N_{\text{ASE}}^2 + 4sN_{\text{ASE}}^3 + N_{\text{ASE}}^4 + N_{\text{th}}^2 + 4sN_{\text{ASE}}N_{\text{th}} + 2N_{\text{ASE}}^2N_{\text{th}}] \\
 &= 4[s^2]E[N_{\text{ASE}}^2] + 4E[s]E[N_{\text{ASE}}^3] + E[N_{\text{ASE}}^4] + E[N_{\text{th}}^2] \\
 &\quad + 4E[s]E[N_{\text{ASE}}]E[N_{\text{th}}] + 2E[N_{\text{ASE}}^2]E[N_{\text{th}}] \\
 &= 4[s^2]E[N_{\text{ASE}}^2] + 4E[s]E[N_{\text{ASE}}^3] + E[N_{\text{ASE}}^4] + E[N_{\text{th}}^2] \\
 &\quad + 4E[s]E[N_{\text{ASE}}]E[N_{\text{th}}] + 2E[N_{\text{ASE}}^2]E[N_{\text{th}}] \\
 &= 4E[s^2]E[N_{\text{ASE}}^2] + E[N_{\text{ASE}}^4] + E[N_{\text{th}}^2]
 \end{aligned}$$

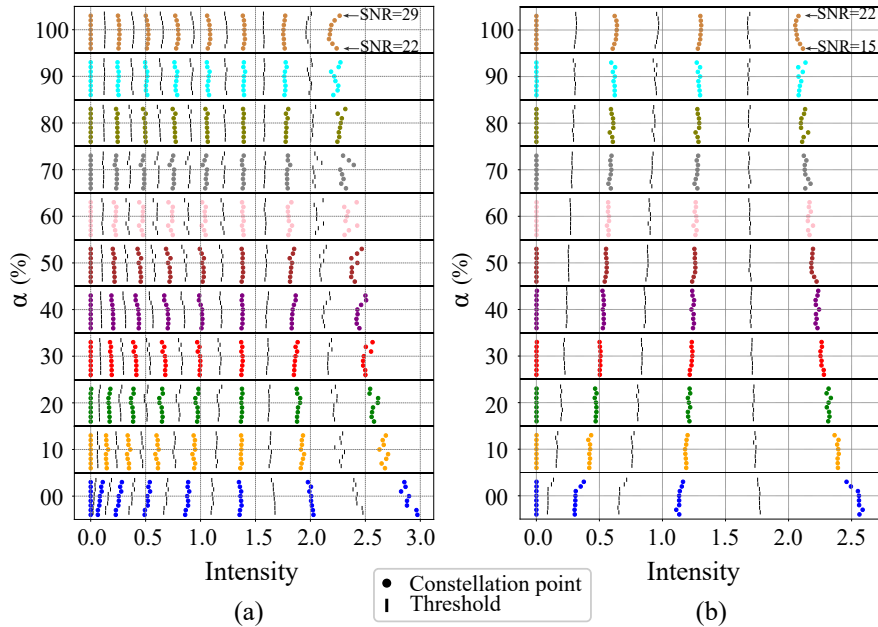


Fig. 11. Constellations and related thresholds for different SNRs for (a) PAM8 and (b) PAM4.

## Appendix B Constellations and thresholds for different SNR values

Fig. 11 illustrates the constellations and thresholds identified for various SNR and  $\alpha$  values. For each  $\alpha$ , eight distinct SNR scenarios are examined, distributed between ASE noise and thermal noise according to the weight of  $\alpha$ . The SNR range is from 22 to 29 dB for PAM8 and from 15 to 22 dB for PAM4. The dependence of both constellation and thresholds on SNR is low.

**Funding.** Natural Sciences and Engineering Research Council of Canada (IRCPJ 546377-18).

**Disclosures.** The authors declare no conflicts of interest.

**Data Availability.** Data underlying the results presented in this paper are randomly generated in Python using random seed and thus, are not included.

## References

1. K. Zhong, X. Zhou, J. Huo, C. Yu, C. Lu, and A. P. T. Lau, "Digital signal processing for short-reach optical communications: A review of current technologies and future trends," *J. Light. Technol.* **36**, 377–400 (2018).
2. R. Rosales, K. Atra, Y. Lin, P. Aivaliotis, G. Berry, X. Chen, M. Gillanders, I. Lealman, D. Moodie, M. Pate, S. Rihani, H. Wang, H. Rongfang, and G. Talli, "50G-PON upstream with over 36dB link budget using an SOA-PIN based receiver," *IEEE Photonics Technol. Lett.* **34**, 1222–1225 (2022).
3. G. Simon, F. Saliou, J. Potet, P. Chanclou, R. Rosales, I. N. Cano, and D. Nasset, "50Gb/s real-time transmissions with upstream burst-mode for 50G-PON using a common SOA pre-amplifier/booster at the OLT," in *2022 Optical Fiber Communications Conference and Exhibition (OFC)*, (2022), pp. 1–3.
4. S. Menezo, Z. Yong, K. Froberger, T. Thiessen, J. C. Mak, F. D.-I. Coarer, M. Peyrou, L. Milord, J. Da Fonseca, C. Jany, P. Grosse, F. Mazur, and J. K. S. Poon, "40GBaud PAM4 silicon mach-zehnder modulator boosted by a heterogeneously integrated SOA with 10dB-gain," in *2022 Optical Fiber Communications Conference and Exhibition (OFC)*, (2022), pp. 1–3.
5. J. K. Perin, M. Sharif, and J. M. Kahn, "Sensitivity improvement in 100 Gb/s-per-wavelength links using semiconductor optical amplifiers or avalanche photodiodes," *J. Light. Technol.* **34**, 5542–5553 (2016).
6. J. Zhang, J. S. Wey, J. Shi, J. Yu, Z. Tu, B. Yang, W. Yang, Y. Guo, X. Huang, and Z. Ma, "Experimental demonstration of unequally spaced PAM-4 signal to improve receiver sensitivity for 50-Gbps PON with power-dependent noise distribution," in *2018 Optical Fiber Communications Conference and Exposition (OFC)*, (IEEE, 2018), pp. 1–3.
7. L. Minelli, F. Forghieri, A. Nespola, S. Straullu, and R. Gaudino, "A multi-rate approach for nonlinear pre-distortion using end-to-end deep learning in IM-DD systems," *J. Light. Technol.* **41**, 420–431 (2023).
8. K. Wang, C. Wang, J. Zhang, Y. Chen, and J. Yu, "Mitigation of SOA-induced nonlinearity with the aid of deep learning neural networks," *J. Light. Technol.* **40**, 979–986 (2022).
9. B. Karanov, M. Chagnon, F. Thouin, T. A. Eriksson, H. Bülow, D. Lavery, P. Bayvel, and L. Schmalen, "End-to-end deep learning of optical fiber communications," *J. Light. Technol.* **36**, 4843–4855 (2018).
10. B. Karanov, G. Liga, V. Aref, D. Lavery, P. Bayvel, and L. Schmalen, "Deep learning for communication over dispersive nonlinear channels: Performance and comparison with classical digital signal processing," in *2019 57th Annual Allerton Conference on Communication, Control, and Computing (Allerton)*, (2019), pp. 192–199.
11. S. Yao, A. Mahadevan, Y. Lefevre, N. Kaneda, V. Houtsma, and D. van Veen, "Artificial neural network assisted probabilistic and geometric shaping for flexible rate high-speed PONs," *J. Light. Technol.* **41**, 5217–5225 (2023).
12. M. Chagnon, B. Karanov, and L. Schmalen, "Experimental demonstration of a dispersion tolerant end-to-end deep learning-based IM-DD transmission system," in *2018 European Conference on Optical Communication (ECOC)*, (2018), pp. 1–3.
13. B. Buscaino, B. D. Taylor, and J. M. Kahn, "Multi-Tb/s-per-fiber coherent co-packaged optical interfaces for data center switches," *J. Light. Technol.* **37**, 3401–3412 (2019).
14. W. Shi, Y. Xu, H. Sepehrian, S. LaRochelle, and L. A. Rusch, "Silicon photonic modulators for PAM transmissions," *J. Opt.* **20**, 083002 (2018).
15. A. G. Reza, M. T. Costas, and L. Barry, "Single-lane 108 Gbit/s C-band PAM-4 transmissions over 1 km using a 40 GHz eam and monolithically integrable SOA-PIN for intra-data center interconnects," in *Advanced Photonics Congress 2023*, (Optica Publishing Group, 2023), p. NeW2B.3.
16. B. Karanov, M. Chagnon, V. Aref, D. Lavery, P. Bayvel, and L. Schmalen, "Concept and experimental demonstration of optical IM/DD end-to-end system optimization using a generative model," in *2020 Optical Fiber Communications Conference and Exhibition (OFC)*, (2020), pp. 1–3.
17. S. Zhalehpour, M. Guo, J. Lin, Z. Zhang, H. Sepehrian, Y. Qiao, W. Shi, and L. A. Rusch, "All silicon IQ modulator with 1Tb/s line rate," in *2020 Optical Fiber Communications Conference and Exhibition (OFC)*, (2020), pp. 1–3.
18. A. M. Gutierrez, A. Brimont, J. Herrera, M. Aamer, D. J. Thomson, F. Y. Gardes, G. T. Reed, J.-M. Fedeli, and P. Sanchis, "Analytical model for calculating the nonlinear distortion in silicon-based electro-optic mach-zehnder modulators," *J. Light. Technol.* **31**, 3603–3613 (2013).